

# Physics-Informed Neural Networks for Nonlocal Beam Eigenvalue Problems

Baidehi Das<sup>a</sup>, Raffaele Barretta<sup>b</sup>, Marko Čanadija<sup>c,\*</sup>

<sup>a</sup>*Department of Civil Engineering and Architecture, University of Catania, Viale Andrea Doria 6, Catania, Italy*

<sup>b</sup>*Department of Structures for Engineering and Architecture, University of Naples Federico II, Via Claudio 21, Naples, 80125, Italy*

<sup>c</sup>*Department of Engineering Mechanics, University of Rijeka, Faculty of Engineering, Vukovarska 58, Rijeka, 51000, Croatia*

---

## Abstract

The present study investigates the dynamics of nonlocal beams by establishing a consistent stress-driven integral elastic using the Physics-Informed Neural Network (PINN) approach. Specifically, a PINN is developed to compute the first eigenfunction and eigenvalue arising from the underlying sixth-order ordinary differential equation. The PINN is based on a feedforward neural network, with a loss function composed of terms from the differential equation, the normalization condition, and both boundary and constitutive boundary conditions. Relevant eigenvalues are treated as separate trainable variables. The results demonstrate that the proposed method is a powerful and robust tool for addressing the complexity of the problem. Once trained, the neural network is less computationally intensive than analytical methods. The obtained results are compared with benchmark analytical solutions and show strong agreement.

**Keywords:** Nonlocal elasticity, Nanobeams, Stress-driven nonlocal model, Physics-Informed Neural Networks, Eigenvalue analysis, Eigenmodes, Higher-order eigenproblems

---



---

\*Corresponding author

Email address: marko.canadija@riteh.uniri.hr (Marko Čanadija)

## 1. Introduction

The design and fabrication of ultrasmall devices such as Micro-Electro-Mechanical Systems (MEMS) and Nano-Electro-Mechanical Systems (NEMS) have a wide range of applications, including energy harvesting [1], novel noise reduction devices [2], healthcare monitoring systems [3], mechanics of advanced materials [4, 5], and innovative structural designs [6, 7]. However, working with these devices at the micro- and nanoscale is challenging, as forces and interactions at the atomistic and molecular levels play a significant role. Although numerous atomistic [8–10] and molecular approaches [11, 12] have been developed, their solutions are often computationally prohibitive. It is important to note that the computational cost can be drastically reduced by combining molecular dynamics, finite elements, and input convex neural networks (see, e.g., [6, 13–15]) in studies of carbon nanotubes. Another way to reduce the computational burden is through nonlocal continuum theories, which began to appear several decades ago [16–18] and were developed for both static and dynamic problems. These nonlocal elasticity theories have successfully captured size effects that conventional local laws fail to describe.

In this context, Eringen [19] adopted a differential constitutive formulation of nonlocal elasticity which has been considered in a variety of contributions, such as [20–22], just to mention a few. In spite of having advantageous implementation of this theory, the latter showed ill-posedness when applied to structural mechanics problems leading to incompatibility between constitutive and equilibrium conditions [23]. To overcome this limitation, a consistent stress-driven integral approach was proposed by [24, 25] which has been successfully applied to various static [26–28] and dynamic [29–31] analytical problems. Nevertheless, despite its robustness, solving complex mechanics problems analytically - particularly those involving higher-order differential formulations - remains challenging.

On the other hand, Neural Networks (NNs) have emerged as powerful tools for addressing complex challenges in structural engineering by modeling nonlinear relationships and processing large datasets. By learning from experimental or simulated data, NNs capture complex nonlinear interactions through interconnected nodes, enabling a wide range of engineering applications. Common types of artificial neural networks (ANNs) include Feedforward Neural Networks (FNNs) and Deep Neural Networks (DNNs), where multiple hidden layers enhance feature extraction for complex tasks. Other architectures, such as Convolutional Neural Networks (CNNs) and Deep Belief Networks (DBNs), have also been employed, particularly for probabilistic structural analysis. Similarly, data-driven techniques

have caught attention for their ability to learn complex patterns and relationships directly from large datasets, enabling predictions in structural engineering tasks without explicit reliance on governing physical equations, see [32–35].

However, data-driven methods and other approaches discussed above often require large datasets, which can pose a significant computational burden [36]. A promising way to mitigate this challenge is to integrate established physical knowledge of the system into the learning process. Such prior physical understanding can be embedded in the training procedure by enforcing the residuals of the governing ordinary or partial differential equations (ODEs or PDEs) at selected training points-effectively incorporating the physical laws into the learning process. This approach, known as Physics-Informed Neural Networks (PINNs), was first introduced in [37].

There are several advantages of PINNs over classical methods for solving differential equations, such as Runge-Kutta or Finite Element/Finite Difference methods:

- In the classical approach, high-dimensional problems are typically solved using basis functions, polynomials, piecewise polynomials, and similar methods. However, these methods are prone to an exponential increase in complexity and computational cost as the number of dimensions grows, a phenomenon commonly referred to as the curse of dimensionality. PINNs, by contrast, have shown greater efficiency in addressing such problems [38], although they also face limitations, particularly when handling higher-order derivatives.
- Unlike classical numerical methods, PINNs do not suffer from the accumulation of numerical errors over time [39], owing to their iterative learning process.
- Ordinary differential equations (ODEs) are typically solved for a fixed set of initial conditions, and changes in those conditions require re-solving the system. PINNs, however, can be designed to handle varying initial conditions without depending on previous solutions [40]. In general, boundary and initial conditions are incorporated into the loss function in PINNs, which makes handling complex conditions significantly easier in challenging cases.
- PINNs can leverage knowledge from related problems. For instance, through transfer learning, a PINN trained on one problem can be efficiently adapted to solve a similar one [41].

- Classical approaches struggle with noisy or incomplete data, a common occurrence in experimental settings [42]. PINNs, however, can incorporate such data more effectively.
- Popular solvers such as the Finite Element Method (FEM) or Finite Difference Method (FDM) often face challenges with mesh generation. PINNs avoid this issue, as they rely only on collocation points, making them inherently mesh-free [42].
- Solving inverse problems using traditional numerical approaches can be computationally prohibitive [42], whereas PINNs provide a more efficient framework for such problems.

On the downside:

- Training PINNs can be slow, and convergence issues often arise.
- Vanishing and exploding gradients pose significant challenges during training.
- Balancing the weights assigned to different loss terms is difficult [43].
- Owing to their iterative nature, PINNs may achieve lower accuracy than classical methods and often require long training times.
- Although the curse of dimensionality is less severe in PINNs compared to classical methods, it still presents challenges. Of particular relevance to structural mechanics is that nonlinear higher-order PDEs involve derivatives of varying orders, which significantly affect the accuracy of automatic differentiation and may lead to convergence issues [44]. This problem arises even in computing second-order derivatives [45] and in classical local beam mechanics governed by fourth-order ODEs. In the present nonlocal case, the governing sixth-order ODE poses an even greater challenge. For these reasons, higher-dimensional problems become especially problematic when higher-order derivatives are involved.

PINNs can also be applied to solving eigenproblems. In this context, they are regarded as an unsupervised forward-inverse technique, where the forward component models the governing differential equation and the inverse component estimates the corresponding eigenvalue. The literature in this area is still relatively limited. For example, [46] proposed an unsupervised PINN algorithm to solve

eigenproblems such as the infinite square well and the quantum harmonic oscillator, both governed by the second-order Schrödinger equation. This method was later improved by incorporating a normalization condition in [47]. More recently, [48] investigated the Schrödinger equation in the context of discovering localized eigenstates. A notable earlier contribution was made by [49], who proposed an ANN framework for solving eigenvalue problems in quantum mechanics. To identify higher-order eigenstates, additional localization loss terms and orthogonality conditions were introduced into the loss function. Another study [50], employed physics-informed dense deep networks and constitutional neural networks to examine eigenmode localization in a class of elliptic reaction-diffusion operators. Furthermore, [51] developed and optimized a deep Gaussian process surrogate model to predict the stability behavior of friction-induced vibration under variability, enabling complex eigenvalue analysis.

For the purposes of the present research, PINN-based eigenanalyses in structural mechanics are particularly relevant. A novel PINN algorithm proposed by [52] computes the natural frequencies of a cantilever beam based on classical mechanics, while addressing convergence issues and the tuning of associated hyperparameters. Similarly, [53] developed a PINN model to capture higher natural frequencies for the free vibration of a three-dimensional functionally graded porous beam resting on an elastic foundation, obtaining benchmark results consistent with analytical solutions. Additionally, [54] applied PINNs to solve both forward and inverse complex beam problems. However, to the best of the authors' knowledge, no studies have yet addressed eigenanalysis for beams exhibiting nonlocal behavior.

Thus, for the first time, the present study proposes a robust PINN algorithm for performing eigenanalysis of nonlocal beams. A consistent stress-driven nonlocal approach is employed to define the underlying differential equation, including the constitutive boundary conditions that arise in nonlocal beams. The proposed PINN methodology computes the first eigenstates of nonlocal cantilever and simply supported beams by solving a sixth-order differential eigenvalue problem, incorporating both standard boundary conditions and constitutive boundary conditions. Additionally, an analysis of the influence of key hyperparameters on the solution is presented.

## **2. Stress-Driven Nonlocal Elasticity for Nonlocal Beams**

Eringen's nonlocal theory of elasticity assumes that the stress at a point depends not only on the elastic strain at that point but also on the elastic strains at

all other points in the structural domain, weighted by an averaging kernel function. However, as mentioned earlier, this theory has shown ill-posedness [23] in structural mechanics problems, showing incompatibility between equilibrium and constitutive requirements. The stress-driven approach on the other hand, circumvents such issues by defining the elastic strain as a nonlocal function of stresses, ensuring well-posedness for a broader range of boundary value problems, especially in nanomechanics.

In this study, a stress-driven nonlocal integral formulation is exploited to study the dynamics of a cantilever nanobeam. According to the stress-driven integral model of elasticity of slender beams, the elastic bending curvature field is the convolution of the local source field  $\frac{M}{K_b}$  and a proper averaging kernel  $\phi_{l_b}$  described by the characteristic length  $l_b$ :

$$\chi^{\text{el}} = \int_0^L \phi_{l_b}(x, \bar{x}) \frac{M}{K_b}(\bar{x}) d\bar{x}. \quad (1)$$

In this regard, a slender Bernoulli–Euler beam of length  $L$  and mass per unit length  $m$  is analyzed under bending, with  $K_b$  denoting the local elastic bending stiffness, and  $M$  the bending moment. The bending occurs in the Cartesian  $(x, y)$ -plane, where the  $x$ -axis aligns with the beam’s longitudinal axis. The deflection function  $w : [0, L] \rightarrow \mathcal{R}$  describes the beam’s transverse displacement. The linearized geometric curvature field  $\chi : [0, L] \mapsto \mathcal{R}$  in terms of the transverse displacement field can be expressed as:

$$\chi = \chi^{\text{el}} + \chi^{\text{nel}} \quad (2)$$

where  $\chi^{\text{el}}$  and  $\chi^{\text{nel}}$  are the elastic and nonelastic parts of the linearized geometric curvature field. The characteristic length  $l_b$  in (1) is defined with the help of a nonlocal parameter  $a$  as  $l_b := aL$ .

The averaging kernel is expressed as the bi-exponential function that fulfills symmetry, positivity and limit impulsivity as:

$$\phi_{l_b}(x) = \frac{1}{2l_b} e^{-\frac{|x|}{l_b}}. \quad (3)$$

Thanks to the properties fulfilled by the special kernel in Eq. (3), the spatial convolution in Eq. (1) can be efficiently inverted providing the following differential equation [23]:

$$\chi(x) - l_b^2 \partial_x^2 \chi(x) = \left( \frac{M}{K_b} \right)(x), \quad (4)$$

equipped with the following constitutive boundary conditions

$$\left\{ \begin{array}{l} \partial_x \chi(0) - \frac{1}{l_b} \chi(0) = 0, \\ \partial_x \chi(0) + \frac{1}{l_b} \chi(0) = 0. \end{array} \right. \quad (5)$$

In Eq. (4), absence of non-elastic effects has been considered, so that the elastic curvature  $\chi^{\text{el}}(x)$  is equal to the geometric one  $\chi(x) := \partial_x^2 w$ , kinematically compatible with the displacement field.

### 3. Dynamic Formulation of Nonlocal Beams

In this section, the free vibration of the nonlocal beam has been addressed with its respective governing differential equation. An Bernoulli-Euler beam is considered having mass linear density defined along the beam axis. As we are considering the free vibration of the nonlocal beam and there is no external loading applied to the system [25], we can write the equilibrium equation for the beam by applying d'Alembert's principle as:

$$\partial_x^2 M(x, t) = -m \partial_t^2 w(x, t). \quad (6)$$

By combining equilibrium with constitutive and kinematic compatibility conditions and assuming spatial uniformity of local bending stiffness  $K_b$ , the following set of differential equations is obtained, id est

$$\left\{ \begin{array}{l} \partial_x^2 M(x, t) = -m \partial_t^2 w(x, t), \\ K_b (\chi(x, t) - l_b^2 \partial_x^2 \chi(x, t)) = M(x, t), \\ \chi(x, t) = \partial_x^2 w(x, t). \end{array} \right. \quad (7)$$

This leads to the sixth-order differential equation:

$$l_b^2 \partial_x^6 w(x, t) - \partial_x^4 w(x, t) + \frac{m}{K_b} \partial_t^2 w(x, t) = 0. \quad (8)$$

The general solution of Eq. (8) can be obtained by using separation of variable methodology to the linearized transverse displacement  $w$  as a product of spatial and temporal functions. Substituting the respective function into Eq. (8) we obtain:

$$l_b^2 \partial_x^6 w(x, t) - \partial_x^4 w(x, t) + \lambda w(x, t) = 0, \quad (9)$$

where  $\lambda = -\frac{m \omega^2}{K_b}$  from which  $\omega$  gives the natural frequency of the system. The derivation of Eq. (9) is proposed in [55].

The subsequent section describes the solution of this sixth-order eigenvalue problem with the help of Physics-Informed Neural Network (PINN).

#### 4. Physics-Informed Neural Network for Nonlocal Beams

Physics-Informed Neural Networks (PINNs) have shown efficiency in solving differential equations [37]. They are a class of machine learning models that incorporate physical laws, typically expressed as differential equations, into the neural network training process. PINNs leverage neural networks to approximate solutions to differential equations while enforcing physical principles (e.g., conservation laws, boundary conditions) as constraints. They combine observational data with the governing equations to ensure that the resulting solutions respect both the data and the underlying physics.

##### 4.1. PINN Methodology

A general overview of the PINN methodology has already been presented in several studies [36, 37, 56]. Therefore, this section outlines the specific strategy for solving eigenvalue problems using the PINN framework.

A typical PINN is a feedforward neural network with multiple hidden layers and suitable activation functions. The inputs are the independent variables (e.g., spatial coordinates  $x$ ), and the outputs represent the dependent variables (e.g., displacement  $w(x)$ ). The network is trained to minimize a loss function that includes contributions from the PDE residual, boundary conditions, and any additional regularization terms. Once the relevant loss components are defined, the neural network is trained using an appropriate optimizer (e.g., the Adam optimizer in this study). During training, the network adjusts the weights and biases of its neurons to minimize the total loss. This minimization process leads to accurate predictions of the underlying physical problem. Automatic differentiation is employed to compute derivatives of the network output, enabling the evaluation of the differential operators required by the governing PDE.

Let us consider a general form of an eigenvalue problem as:

$$\mathcal{L}w(x) + \lambda w(x) = 0 \quad (10)$$



where  $\mathcal{L}$  is a differential operator,  $w$  is the eigenfunction, and  $\lambda$  is the associated eigenvalue. After feeding on the input into suitable hidden layers using relevant activation function, losses are computed. As we are interested in computing eigenvalues and corresponding eigenfunctions of the system, the total loss is typically defined [52] as:

$$L_{\text{tot}} = \alpha_{\text{de}} L_{\text{de}} + \alpha_{\text{bc}} L_{\text{bc}} + \alpha_{\text{cbc}} L_{\text{cbc}} + \alpha_{\text{nor}} L_{\text{nor}}, \quad (11)$$

where  $L_{\text{de}}$  is the differential equation loss,  $L_{\text{bc}}$  and  $L_{\text{cbc}}$  enforce the boundary conditions and constitutive boundary conditions, and  $L_{\text{nor}}$  is the normalization or regularization term. These individual losses are multiplied by corresponding weighting factors  $\alpha_{\bullet}$  in order to better emphasize each of the above terms.

An important point regarding the definition the normalization should be noted. [46] initially proposed a regularization loss term which was given as the summation of losses as shown in Eq. (12) below, scaled by respective weight factor. The two losses of interest with the role to penalize convergence to trivial solutions were:

$$L_{\text{nor}} = L_{\text{f}} + L_{\lambda}, \quad L_{\text{f}} = w(x)^{-2}, \quad L_{\lambda} = \lambda^{-2}, \quad (12)$$

where  $w$  is the predicted eigenfunction, and  $\lambda$  is the eigenvalue. Therefore, we initially adopted Eq. (12) but PINN was not being able to converge to the correct eigenstate. Investigating on this context, [47] noted that while the numerical trick in Eq. (12) tends to penalize trivial solutions, it lacks a physical basis. Moreover, small eigenvalues and eigenfunction close to  $w(x) = 0$  lead toward infinite values of the loss function, and consequently cause convergence issues. This formulation was updated in [47, 48] with additional conditions that address these issues. The regularization term is thus proposed in the form of a normalization loss:

$$L_{\text{nor}} = \left( \int_0^L w^2(x) dx - 1 \right)^2, \quad (13)$$

where  $w$  is the predicted eigenfunction, and the integral is taken over the interval  $[0, 1]$ . Application of the midpoint rule provides an approximation as:

$$L_{\text{nor}} \approx \left( \sum_{i=1}^{N_c-1} (w_m)_i^2 - \frac{1}{\Delta x} \right)^2, \quad (14)$$

where  $dx \approx \Delta x = (N_c - 1)/L$ ,  $N_c$  is the number of collocation points, and  $(w_m(x_m))_i$  are the values of the eigenfunction  $w(x)$  evaluated at the midpoints

$(x_m)_i$  between two neighboring collocation points. We adopted the same approach, which significantly reduced the numerical error and enabling the convergence of the loss term to zero, enabling accurate prediction of the eigenvalue and eigenfunction.

After defining the respective loss terms, the neural network model is trained using a suitable optimizer, preferably the Adam optimizer [47, 48, 52]. It is also important to consider the tuning of hyperparameters, such as the number of neurons in dense layers, learning rates, weighting factors for the loss terms, and the choice of activation functions, as these significantly affect the model's training. The optimal adjustment of hyperparameters can vary depending on the problem. However, these aspects are discussed in detail in the case-study sections of this article.

## 5. Case Study 1: PINN for Local Cantilever Eigenvalue Problem

### 5.1. Structural Problem Formulation

The proposed PINN methodology has been first implemented to solve the eigenvalue problem of a local cantilever beam, as illustrated in Fig. 1, to determine the first eigenvalue and its corresponding eigenfunction. Since the local problem is governed by a fourth-order differential equation, its approximation using a PINN requires significantly less computational effort compared to the nonlocal case. Therefore, the selection of the PINN architecture and other relevant hyperparameters is performed on the local problem using a trial-and-error approach, which serves as a basis for subsequent fine-tuning in the nonlocal PINN formulation.

All beams analyzed in this study have a unit length and a unit square cross-section, with length, width, and height each set to unity. Since no specific materials are assigned to the structural schemes, the combination of geometric and material parameters,  $\frac{m}{K_b}$ , is also taken as 1. In the local case, the governing equation is a fourth-order differential equation, as shown in Eq. (9) with  $l_b = 0$ :

$$-\partial_x^4 w + \lambda w = 0, \quad x \in [0, L], \quad (15)$$

and the beam is subjected to its respective kinematic boundary conditions at  $x = 0$  and at  $x = L$ :

- Clamped at  $x = 0$ :

$$w(0) = 0, \partial_x w(0) = 0. \quad (16)$$

- Free at  $x = L$ :

$$M(L) = \partial_x^2 w(L) = 0, \partial_x M(L) = \partial_x^3 w(L) = 0. \quad (17)$$

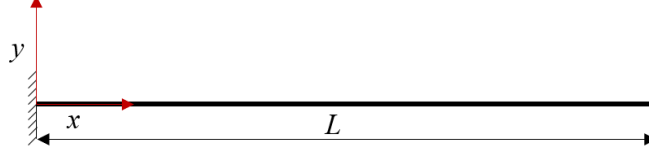


**Fig. 1.** Schematic of Nonlocal Cantilever Beam

The PINN approach is implemented to approximate the eigenfunction  $w$  and the eigenvalue  $\lambda$ , that correspond to the square of the natural frequency  $\omega$ .

### 5.2. PINN Architecture and Training

In all cases considered in the present research, we adopted a PINN model, as shown in Fig. 2, consisting of two components: a neural network to approximate the eigenfunction  $w$  and a trainable variable representing the eigenvalue  $\lambda$ . The neural network consists of three dense layers with 128, 64, and 32 neurons, respectively, using the swish activation function

$$f(x) = x \cdot \sigma(\beta x), \quad \text{where} \quad \sigma(\beta x) = (1 + \exp(-\beta x))^{-1}, \quad \beta = 1 \quad (18)$$

in the hidden layers, [57]. While activation functions such as hyperbolic tangent, ReLU, softplus, sine, and sigmoid are commonly used in PINNs, we observed that the swish activation function significantly improved the accuracy of eigenstate prediction. This finding is consistent with reports in the literature [58], which attribute the improvement to swish's ability to mitigate the vanishing gradient problem. Although the ReLU activation function was successfully applied to the second-order problem in [48], it is not expected to be a suitable choice for the sixth-order problem at hand due to the absence of higher-order derivatives. The hyperbolic tangent activation function has been used in the classical cantilever beam eigenvalue fourth-order problem. The sine function was employed in [46, 47], where superior performance compared to the hyperbolic tangent and sigmoid functions was reported. Bias vectors were not used in the network, and all layers employed the Glorot uniform initializer for weight initialization. In the initial phase of the research, random seeds were fixed in TensorFlow to ensure reproducibility; in later stages, random seeds were not fixed, but the performance remained consistent.

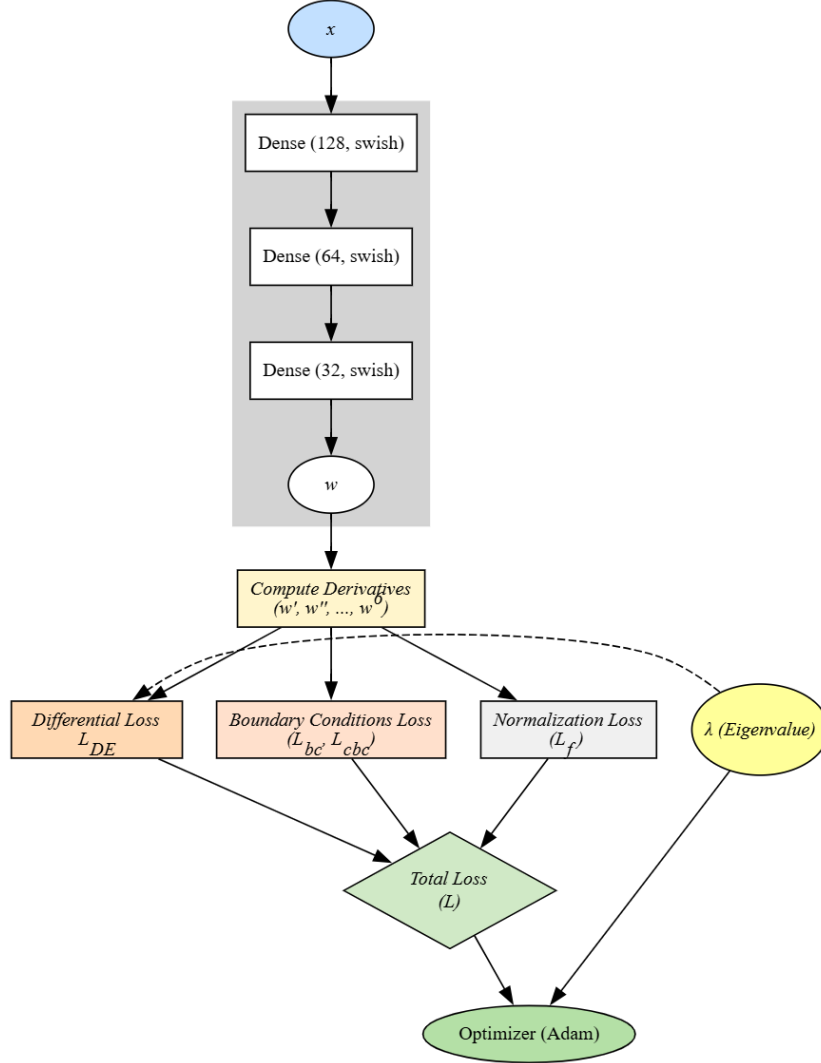


**Fig. 2.** PINN Architecture

The Adam optimizer was employed with a relatively large constant learning rate of  $10^{-2}$ , and an L2 regularization penalty of  $10^{-6}$  was applied.

We generate 100 uniformly spaced collocation points in  $x \in [0, 1]$  for the cantilever beam to evaluate the differential equation residual and boundary conditions. A specific initial value of  $\lambda$  is provided, which gradually adjusts itself during training to attain the desired eigenvalue.

The model is trained for a given number of epochs, updating weights and  $\lambda$  at

No. epochs	30 000
Initial $\lambda$	100.0000
Predicted $\lambda$	12.4581
Analytical $\lambda$	12.3596
Difference (%)	-0.7972
min. $L_{\text{tot}}$	0.05489

**Table 1.** Number of training epochs, initial, predicted, analytical value of  $\lambda$ , and difference, total loss for a high learning rate case applied to a local cantilever beam.

each epoch. The training loop computes fourth-order derivatives using automatic differentiation via `tf.GradientTape`, and evaluates the loss components  $L_{\text{de}}$ ,  $L_{\text{bc}}$ , and  $L_{\text{nor}}$ . The weighting factors for the losses were set as  $\alpha_{\text{de}} = 1$ ,  $\alpha_{\text{bc}} = 100$ , and  $\alpha_{\text{nor}} = 5$ . During the adjustment of weighting factors by trial-and-error, it was observed that larger weights for boundary conditions facilitate training. The scaling factor  $\alpha_{\text{de}}$  applied to the loss is kept at 1, signifying that this loss component is neither amplified nor diminished relative to the other components in the total loss history. Model weights and training state are saved at each new minimum of the total loss. After training, the final eigenfunction  $w$  is normalized such that  $w(L) = 1$ .

### 5.3. Results and Discussion

The main results are presented in Tab. 1 and Fig. 3. It is noteworthy that, although the initial value of  $\lambda$  differs considerably from the analytically obtained eigenvalue, the PINN is still able to converge to the correct solution. Compared to other authors [47, 48, 52], who used learning rates of  $1 \times 10^{-3}$ ,  $8 \times 10^{-3}$ , and  $5 \times 10^{-4}$  for less demanding problems than the current one, the constant high learning rate of  $10^{-2}$  employed here - for both  $\lambda$  and the network weights - demonstrated robust training performance. It successfully captured the correct first eigenvalue and eigenfunction, albeit at the cost of slightly reduced accuracy. To further investigate the training behavior under lower and adaptive learning rate, an additional analysis is conducted and documented in [Appendix A](#).

## 6. Case Study 2: PINN for Nonlocal Cantilever Beam Eigenvalue Problem

### 6.1. Structural Problem Formulation

In this case study, the eigenstate of a nonlocal cantilever beam is considered. The governing equation has already been presented in Eq. (9), and the nonlocal

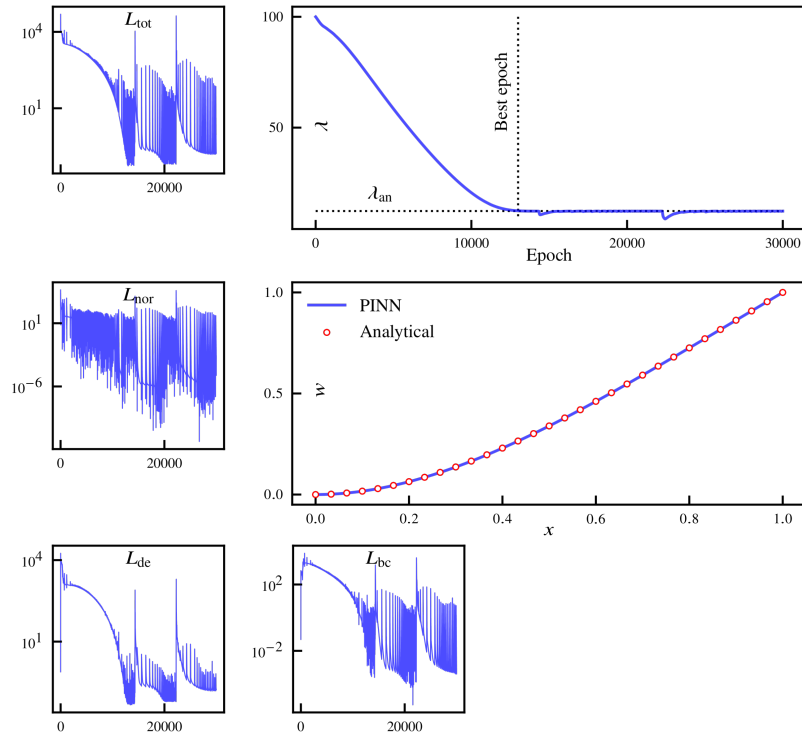


**Fig. 3.** Local cantilever beam with high learning rate:  $\lambda$  convergence, first eigenfunction, and loss histories.

parameter is taken as  $a = 0.1$ . Therefore, based on the relation between the characteristic length and the actual length described above,  $l_b$  is also equal to 0.1 for a unit actual length  $L = 1$ . The boundary conditions for the nonlocal cantilever beam include both the constitutive boundary conditions, as defined in Eq. (5), and the usual kinematic boundary conditions. These can be listed as:

- Clamped at  $x = 0$ :

$$\begin{aligned} w(0) &= 0 \\ \partial_x w(0) &= 0 \\ \partial_x^3 w(0) - \frac{1}{l_b} \partial_x^2 w(0) &= 0. \end{aligned} \quad (19)$$

- Free at  $x = L$ :

$$\begin{aligned} M(L) &= \partial_x^2 w(L) - l_b^2 \partial_x^4 w(L) = 0 \\ \partial_x M(L) &= \partial_x^3 w(L) - l_b^2 \partial_x^5 w(L) = 0 \\ \partial_x^3 w(L) + \frac{1}{l_b} \partial_x^2 w(L) &= 0. \end{aligned} \quad (20)$$

It should also be noted that the values of  $\lambda$  correspond to the eigenvalues of the problem, and the natural frequency  $\omega$  can be computed as square root of  $\lambda$ , since the other material and geometric parameters are taken as unity in the present case.

## 6.2. Design of Loss Functions

As mentioned in Sec. 4.1, appropriately defining the loss functions plays a crucial role in training the neural network to solve differential equations by embedding physical laws and constraints directly into the optimization process. Below is a concise explanation of the different types of loss functions used in our PINN model, including the differential equation loss  $L_{de}$ , kinematic boundary loss  $L_{bc}$ , constitutive boundary loss  $L_{cbc}$ , and normalization loss  $L_{norm}$ .

- Differential Equation Loss ( $L_{de}$ ):

$$L_{de} = \left[ \frac{1}{N_c} \sum_{i=1}^{N_c} \left( l_b^2 \partial_x^6 w(x_i) - \partial_x^4 w(x_i) + \lambda w(x_i) \right)^2 \right] \quad (21)$$

The loss  $L_{de}$  represents the squared residual of the differential equation evaluated at each collocation point  $x_i$ . The residual quantifies how well a candidate solution  $w(x)$  satisfies the differential equation. The factor

$\frac{1}{N_c}$  normalizes the sum of squared residuals by the number of collocation points, ensuring that the loss represents an average and is independent of the discretization density. This normalization allows for consistent comparisons across different sets of collocation points. The summation  $\sum_{i=1}^{N_c}$  aggregates the squared residuals at all collocation points, with the index  $i$  running from 1 to  $N_c$ , so that the loss evaluates the differential equation's residual at  $N_c$  distinct points.

- Boundary Condition Losses ( $L_{bc}$ ):

$$L_{bc} = w(0)^2 + (\partial_x w(0))^2 + \left( \partial_x^2 w(L) - l_b^2 \partial_x^4 w(L) \right)^2 + \left( \partial_x^3 w(L) - l_b^2 \partial_x^5 w(L) \right)^2, \quad (22)$$

The total kinematic boundary condition loss is computed as the mean of the squared terms for all kinematic boundary conditions.

- Constitutive Boundary Condition Loss ( $L_{cbc}$ ):

$$L_{cbc} = \left[ \left( \partial_x^3 w(0) - \frac{1}{l_b} \partial_x^2 w(0) \right)^2 + \left( \partial_x^3 w(L) + \frac{1}{l_b} \partial_x^2 w(L) \right)^2 \right], \quad (23)$$

- Normalization Loss ( $L_{norm}$ ): As discussed in Sec. 4.1, the normalization loss has been defined in Eq. (14) as:

$$L_{norm} = \left( \sum_{i=1}^{N_c-1} (w_m)_i^2 - \frac{1}{\Delta x} \right)^2. \quad (24)$$

During training, it was observed that the scaling factor for the regularization loss plays a crucial role in both the loss and eigenvalue convergence. Therefore, it can be considered an important hyperparameter.

The total loss is computed using the weighting factors defined in Eq. (11). The contributions of the individual loss terms and their corresponding weights have been carefully tuned to ensure favorable convergence and accuracy of both the eigenvalue and the eigenfunction. The specific values for these weights are the same as those used in the local case, as described in Sec. 5.2 with the addition of  $\alpha_{cbc} = 100$ . Similarly, all other hyperparameters remain unchanged from the local case.



L2	None	$10^{-4}$	$10^{-6}$
Best epoch	49 578	23 322	49 774
Best $\lambda$	14.8844	15.0812	15.1236
min. $L_{\text{tot}}$	0.8070	1.88343	0.5357

**Table 2.** Influence of L2 regularization on PINN training for 50 000 epochs. Analytical result  $\lambda_{\text{an}} = 15.1953$ .

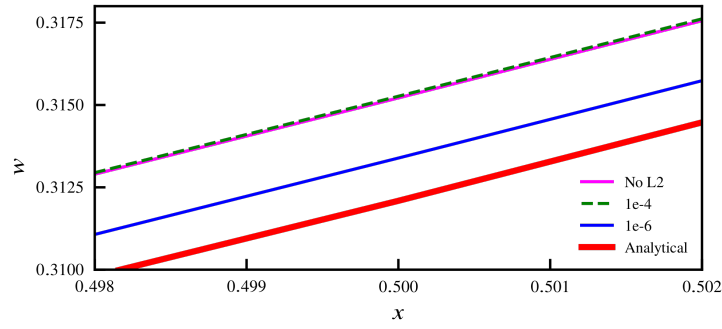


**Fig. 4.** Influence of L2 regularization on PINN training - central part of the first eigenfunction curve. Colors: magenta - no L2 regularization, green - regularization value  $10^{-4}$ , blue - regularization value  $10^{-6}$ , red - analytical solution.

### 6.3. Preliminary Investigation

In the preliminary stage, the influence of selected hyperparameters, previously determined for the local case, was re-examined for the nonlocal cantilever beam.

The first set of analyses examines the influence of the L2 regularization penalty applied to each dense layer. Gradient clipping on the training variables was not employed. As evident from Tab. 2 and Fig. 4, an L2 penalty of  $10^{-6}$  yields the best results for both  $\lambda$  and the total loss after training for 50 000 epochs. In contrast, the absence of L2 regularization produces the poorest approximation of the first eigenvalue. Similarly, for the case  $10^{-4}$ , the best result occurs at epoch 23 322, after which no further improvement is observed, unlike the other cases. For these reasons, the penalty value  $10^{-6}$  is adopted in all subsequent analyses.

The second set of analyses focused on the effect of gradient clipping on PINN training. Four cases were considered:

1.  $\lambda$  gradient clipped by value to remain in the range  $[-1, 1]$ , while gradients of the remaining NN weights were clipped by L2-norm at 1.0 (denoted as

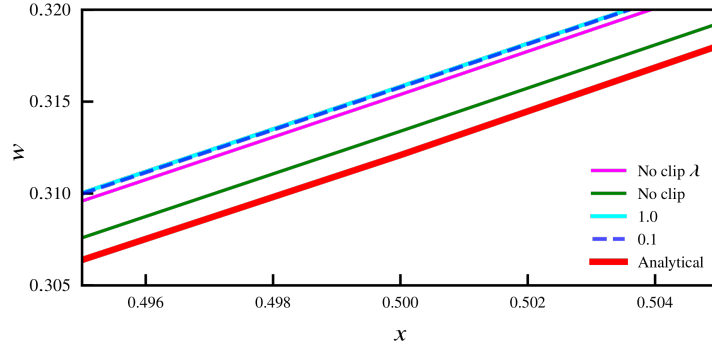


**Fig. 5.** Influence of gradient clipping on PINN training: central part of the first eigenfunction curve. Colors: green - no gradient clipping, magenta - no gradient clipping for  $\lambda$  and NN weights gradients clipping value 1.0, cyan - clipping value 1.0, blue/dashed - clipping value 0.1, red - analytical solution.

1.0 in Fig. 5).

2.  $\lambda$  gradient clipped by value to remain in the range  $[-1, 1]$ , while gradients of the remaining NN weights were clipped by L2-norm at 0.1 (denoted as 0.1).
3.  $\lambda$  gradient not clipped, while gradients of the remaining NN weights were clipped by L2-norm at 1.0 (denoted as No clip  $\lambda$ ).
4. Neither  $\lambda$  nor weights gradients were clipped (denoted as No clip).

Part of the results is shown in Fig. 5 and Tab. 3. In all cases, the same random initial weights were used, and an L2 regularization penalty of  $10^{-6}$  was applied in each dense layer. It is evident that when gradients were not clipped (No clip, case 4 above), the value of  $\lambda$  closest to the analytical solution was obtained, although the total loss was slightly worse than in case 1.0 (case 1 above). However, the most accurate eigenfunction was again observed in case 4 (No clip), Fig. 5. From Tab. 3, it is also clear that in the No clip  $\lambda$  case, the lowest loss is obtained relatively early (epoch 37 958), after which the optimizer is unable to progress further. A similar conclusion can be drawn for the remaining cases where gradient clipping was applied, although the effect is less pronounced. When gradient clipping is not used (No clip case), the optimizer is able to progress throughout the training and would most likely continue to improve further if more epochs were allowed. Consequently, no gradient clipping was adopted for the main calculations presented in the next section.

The third and final set of investigations concerns the choice of activation

Case	1.0	0.1	No clip $\lambda$	No clip
Best epoch	43 800	46 635	37 958	49 774
Best $\lambda$	15.049	15.037	14.869	15.124
min. $L_{\text{tot}}$	0.515	0.874	1.269	0.535

**Table 3.** Influence of gradient clipping on PINN training for 50 000 epochs. Analytical result  $\lambda_{\text{an}} = 15.1953$ .

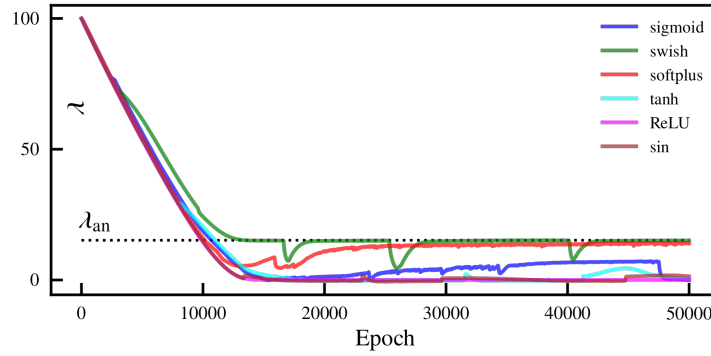


**Fig. 6.** Effect of the choice of activation function on  $\lambda$

function. As previously mentioned, hyperbolic tangent, ReLU, softplus, sine, sigmoid, and swish activation functions were considered. The convergence of  $\lambda$  during training is shown in Fig. 6. It is clear that the swish activation function is by far the most effective choice, while the only viable alternative could be the softplus function, although it exhibits a lower convergence rate. The sigmoid activation function may yield a similar result, but with significantly poorer convergence. Regarding the effect on the first eigenmode, shown in Fig. 7, the same conclusions can be drawn. Differently to [46–48, 52], hyperbolic tangent, ReLU, and sine functions do not provide an appropriate shape of the curve, although the boundary conditions are correctly satisfied. In contrast, the softplus and sigmoid functions approximately capture the correct shape of the eigenmode, but they fail to satisfy the boundary conditions within the given number of epochs.

#### 6.4. Results and Discussion

Based on the above results, no gradient clipping was applied to any trainable variables in the final analysis, while an L2 regularization penalty of  $10^{-6}$  was

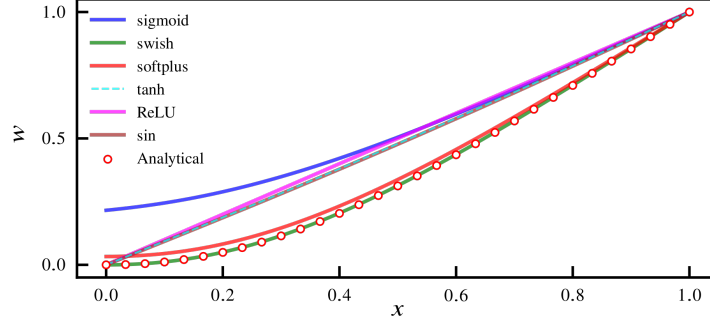


**Fig. 7.** Effect of the choice of activation function on the first eigenmode

No. epochs	50 000
Initial $\lambda$	100.0000
Predicted $\lambda$	15.1182
Analytical $\lambda$	15.1953
Difference (%)	0.5074
min. $L_{\text{tot}}$	0.5144

**Table 4.** Number of training epochs, initial, predicted, analytical value of  $\lambda$ , and difference, total loss for a high learning rate for a nonlocal cantilever beam.

used. The results are presented in Tab. 4 and Fig. 8 for a high constant learning rate of  $10^{-2}$ . This higher learning rate enables more robust training; even when the initial guess for the eigenvalue ( $\lambda_{\text{ini}} = 100$ ) is far from the analytical value ( $\lambda_{\text{an}} = 15.1953$ ), the correct eigenvalue is obtained. To illustrate training results for a lower and adaptive learning rate, an additional training is performed and results are documented in [Appendix A](#).

During numerical experimentation, the higher learning rate also showed less sensitivity to suboptimal choices of parameters and procedures (e.g., loss weights, L2 regularization, gradient clipping) compared to low and adaptive learning rates. This was primarily reflected in the failure of the lower learning rates to converge to the correct  $\lambda$ , although obtaining the first eigenfunction was less problematic. Training results for the low and adaptive learning rates are documented in [Appendix A](#), particularly in Fig. A.12. It is evident that lower learning rates yield more accurate results, albeit at significantly increased computational cost.

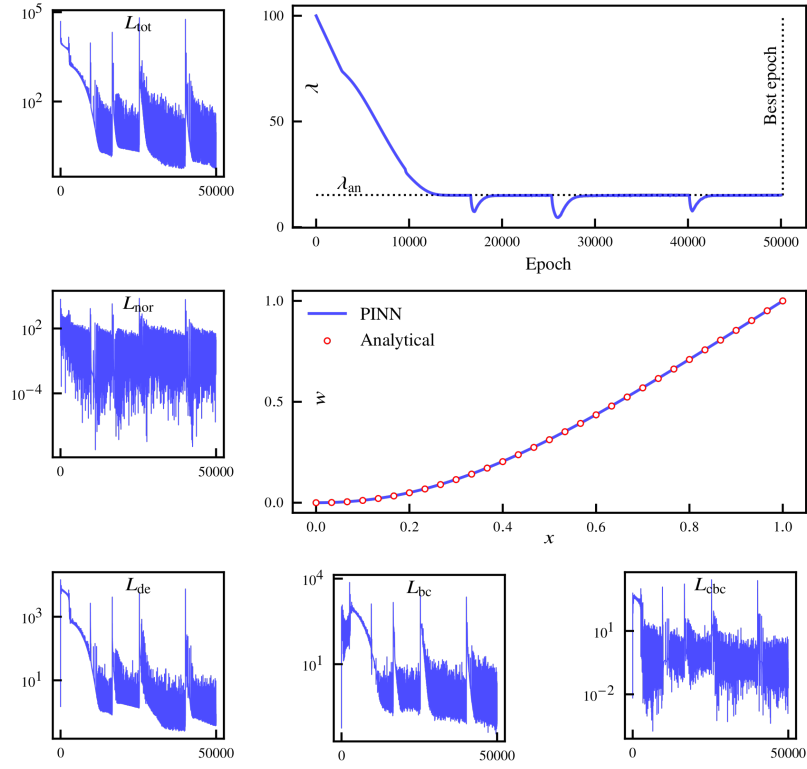


**Fig. 8.** Nonlocal cantilever beam with a high learning rate:  $\lambda$  convergence, first eigenfunction, and loss histories.

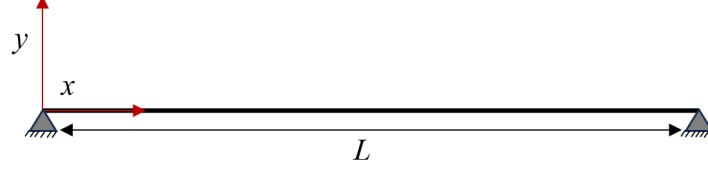


**Fig. 9.** Schematic of Nonlocal Simply Supported Beam

### 7. Case Study 3: PINN for Nonlocal Simply Supported Beam Eigenvalue Problem

The final case considers the determination of the eigenstate for a nonlocal simply supported beam, as shown in Fig. 9. All parameters and settings remain the same as for the nonlocal cantilever beam described in Sec. 6, except for the boundary condition loss, which now takes the following form:

$$L_{bc} = w(0)^2 + \left( \partial_x^2 w(0) - l_b^2 \partial_x^4 w(0) \right)^2 + w(L)^2 + \left( \partial_x^2 w(L) - l_b^2 \partial_x^4 w(L) \right)^2. \quad (25)$$

The number of collocation points in this case is taken to be  $N_c = 101$  in order to include a point at the midspan of the beam, which is used for normalization of the eigenfunction.

#### 7.1. Results and Discussion

For the present case, the results are summarized in Tab. 5 and Fig. 10. The same conclusions drawn for the nonlocal cantilever beam apply to the nonlocal simply supported beam. Once again, the training is robust and converges to the analytically obtained eigenstate. The problem is revisited using lower and adaptive learning rates in Appendix A. During the trial-and-error process, it was again observed that the lower and adaptive learning rates are more sensitive to the choice of hyperparameters.

## 8. Conclusions

For the first time, this study presents a robust application of Physics-Informed Neural Networks (PINNs) to address the eigenvalue problem associated with the

No. epochs	80 000
Initial $\lambda$	150.000
Predicted $\lambda$	104.496
Analytical $\lambda$	105.133
Difference (%)	0.6059
min. $L_{\text{tot}}$	0.1042

**Table 5.** Number of training epochs, initial, predicted, analytical value of  $\lambda$ , and difference, total loss for a high learning rate for the nonlocal simply supported beam.

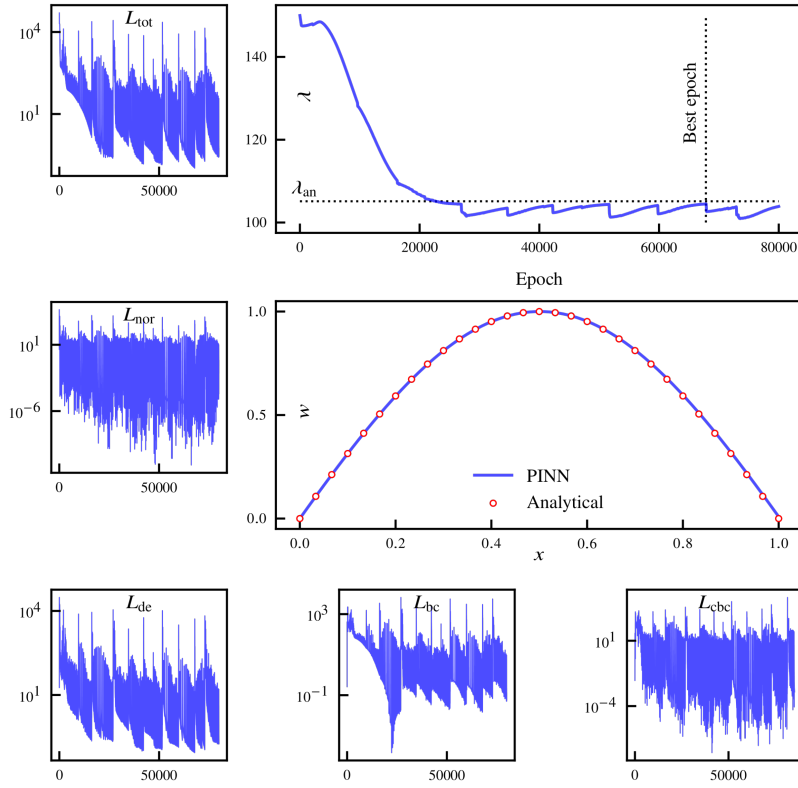


**Fig. 10.** Nonlocal simply supported beam with a high learning rate:  $\lambda$  convergence, first eigenfunction, and loss histories.

free vibration of nonlocal cantilever and simply supported beams, as well as a local cantilever beam, for the determination of their first eigenvalues. As a preliminary step, the local problem was solved to efficiently obtain suitable hyperparameters, which were then reused for the nonlocal problem. By leveraging the stress-driven nonlocal model, the governing sixth-order differential equation was formulated and the forward - inverse problem was solved using a PINN architecture that integrates the governing physical laws, along with kinematic and constitutive boundary conditions, directly into the loss function. The proposed methodology demonstrates high accuracy in predicting both the eigenvalues and corresponding eigenfunctions, achieving excellent agreement with analytical solutions across all considered structural configurations.

The PINN approach offers significant advantages over traditional analytical and numerical methods, particularly in handling complex differential equations without the need for mesh generation or computationally intensive procedures. The use of the swish activation function, carefully tuned hyperparameters, and a composite loss function incorporating differential equation residuals, boundary conditions, constitutive boundary conditions, and normalization terms ensured stable convergence and precise predictions. On the downside, the determination of sixth-order derivatives via automatic differentiation is relatively slow and significantly prolongs the training process. However, once trained - as is typically the case with neural networks - the evaluation of the eigenstate is very fast.

### **Data availability**

An example of code used in this research can be found at Das, Baidehi; Barretta, Raffaele; Čanadija, Marko (2025), "PINN for Nonlocal Beam Eigenvalue Problems", Mendeley Data, V1, doi: 10.17632/7hf2v6r237.1

### **Acknowledgments**

This work was supported by the University of Rijeka under project uniri-mzi-25-16 and Financial support from the Italian Ministry of University and Research (MUR) in the framework of the Project PRIN 2022 PNRR code P20223PLC2 "Nonlocal modelling of nano-coatings" is gratefully acknowledged.

### **Appendix A. Results Obtained Using Lower and Adaptive Learning Rate**

In the following cases, exponential decay learning rates are used: one for neural network weights (initial rate  $5 \times 10^{-4}$ , decay steps 5 000, decay rate 0.9) and one



	L CF	NL CF	NL SS	NL SS
No. epochs	50 000	150 000	150 000	300 000
Initial $\lambda$	14	16	106	106
Predicted $\lambda$	12.3576	15.1813	105.088	105.111
Analytical $\lambda$	12.3596	15.1953	105.133	105.133
Difference (%)	0.016	0.092	0.043	0.021
min. $L_{\text{tot}}$	0.005068	0.07833	0.12374	0.06292

**Table A.6.** Number of training epochs, initial, predicted, and analytical values of  $\lambda$ , difference, and total loss for a low and adaptive learning rate for a local cantilever beam (L CF), nonlocal cantilever beam (NL CF), and nonlocal simply supported beam (NL SS). For the simply supported beam, results for the same training at 150 000 and 300 000 epochs are reported.

for  $\lambda$  (initial rate  $1 \times 10^{-4}$ , with the same decay parameters). For the nonlocal problems, the decay steps parameter was increased to 25 000.

The results are summarized in Tab. A.6 and Figs. A.11, A.12, and A.13 for the local cantilever beam, nonlocal cantilever beam, and nonlocal simply supported beam, respectively. For comparison, results for the simply supported beams at 150 000 and 300 000 epochs are also reported in Tab. A.6. All other hyperparameters were kept identical to those used in the high learning rate case. It is evident that the local cantilever beam requires the fewest epochs to converge. For the nonlocal beams, the cantilever beam achieves a lower total loss after 150 000 epochs compared to the simply supported beam, although the difference in the predicted eigenvalues is larger for a cantilever beam. Both nonlocal beams exhibit relatively low loss at the end of training, and  $\lambda$  can be obtained even closer to the analytical value if training is continued for additional epochs.

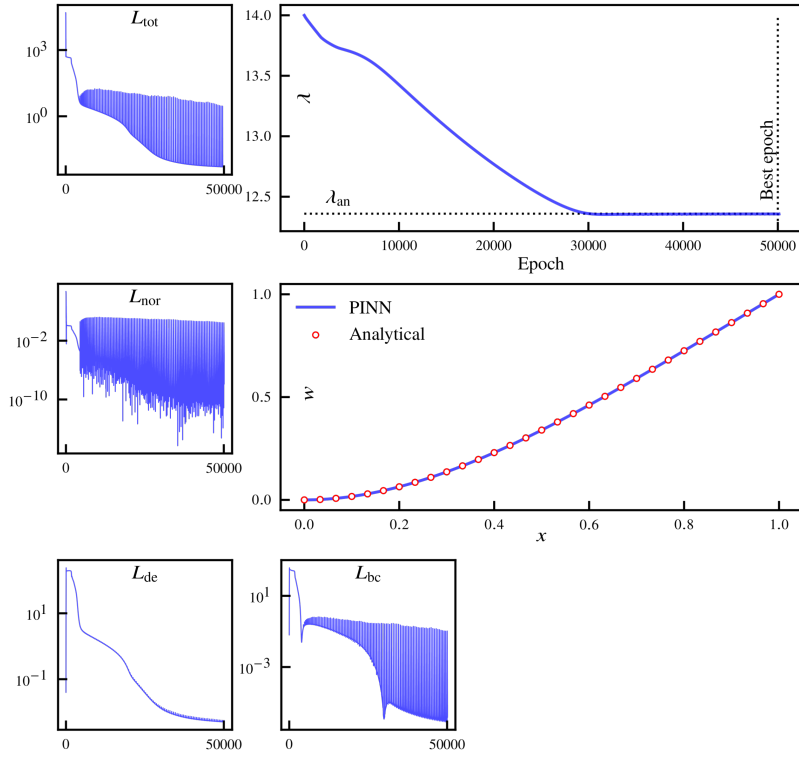


**Fig. A.11.** Local cantilever beam with low and adaptive learning rate:  $\lambda$  convergence, first eigenfunction and loss histories.

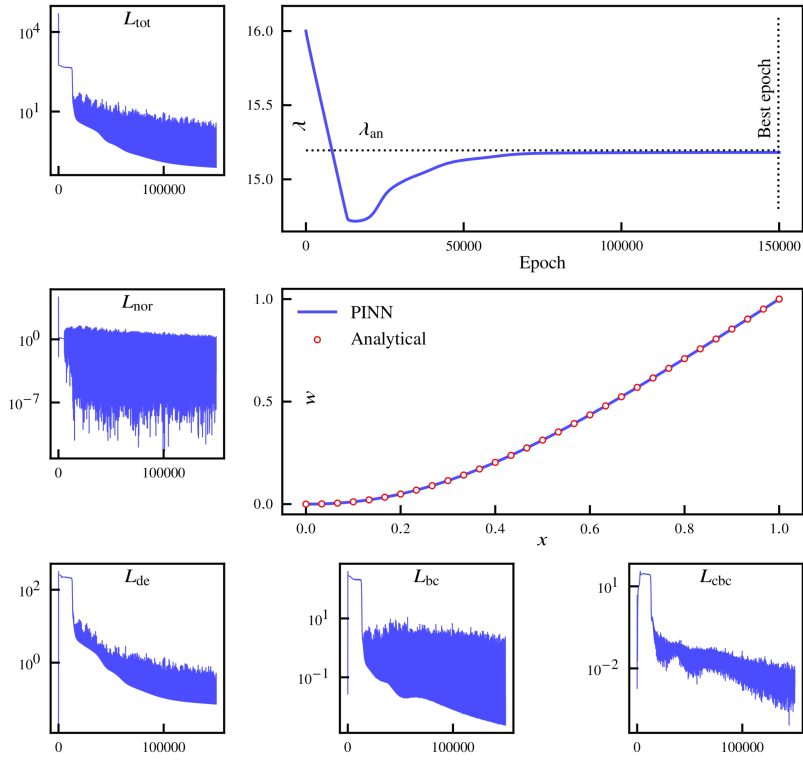


**Fig. A.12.** Nonlocal cantilever beam with low and adaptive learning rate:  $\lambda$  convergence, first eigenfunction and loss histories.

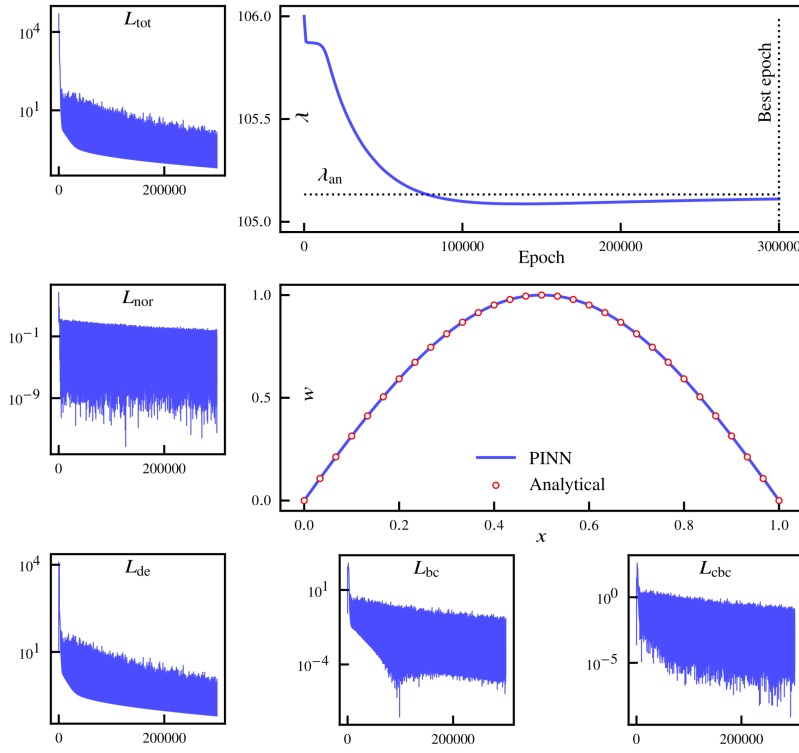


**Fig. A.13.** Nonlocal simply supported beam with low and adaptive learning rate:  $\lambda$  convergence, first eigenfunction and loss histories.

## References

- [1] Z. Ren, S. Deng, J. Shao, Y. Si, C. Zhou, J. Luo, T. Wang, J. Li, J. Li, H. Liu, X. Qi, P. Wang, A. Yin, L. Wu, S. Yu, Y. Zhu, J. Chen, S. Das, J. Wei, Z. Chen, Ultrahigh-power-density flexible piezoelectric energy harvester based on freestanding ferroelectric oxide thin films, *Nature Communications* 16 (1) (2025) 3192.
- [2] T. Lu, W. Zheng, R. Tang, L. Li, Beam-type acoustic black holes incorporating the microstructure-dependent nonlocal effect, *Thin-Walled Structures* 197 (2024) 111662.
- [3] V. Abhinav, P. Basu, S. S. Verma, J. Verma, A. Das, S. Kumari, P. R. Yadav, V. Kumar, Advancements in wearable and implantable BioMEMS devices: Transforming healthcare through technology, *Micromachines* 16 (2025).
- [4] R. Izadi, R. Das, N. Fantuzzi, P. Trovalusci, Fracture properties of green nano fibrous network with random and aligned fiber distribution: A hierarchical molecular dynamics and peridynamics approach, *International Journal of Engineering Science* 204 (2024).
- [5] B. Yang, N. Fantuzzi, M. Baccocchi, F. Fabbrocino, M. Mousavi, Nonlinear wave propagation in graphene incorporating second strain gradient theory, *Thin-Walled Structures* 198 (2024).
- [6] M. Čanađija, S. Ivić, Carbon nanotubes as a basis of metamaterials and nanostructures: Crafting via design optimization, *Mechanics of Materials* 197 (2024) 105105. doi:<https://doi.org/10.1016/j.mechmat.2024.105105>.
- [7] A. Gabrelian, V. Miikkulainen, G. Ross, M. Paulasto-Kröckel, Scaling of piezoelectric in-plane NEMS: Towards nanoscale integration of AlN-based transducer on vertical sidewalls, *Materials & Design* 244 (2024) 113116.
- [8] V. K. Choyal, R. S. Kumar, S. I. Kundalwal, Vibrational behavior of stacked boron nitride/graphene heterogeneous layers: A comprehensive atomistic simulation study, *Journal of Vibration Engineering & Technologies* 13 (5) (2025) 352.
- [9] A. Moradi, H. M. Sedighi, M. Shishesaz, A. Ghanbarzadeh, H. Ameri, Calibration of size-dependent vibrations of aluminum and silver nanobeams by

means of hybrid atomistic-continuum simulations using molecular dynamics in conjunction with bees algorithm, *The European Physical Journal Plus* 140 (3) (2025) 189.

- [10] V. Kushch, Atomistic and continuum modeling of nanoparticles: Elastic fields, surface constants, and effective stiffness, *International Journal of Engineering Science* 183 (2023) 103806.
- [11] L. Najmi, Z. Hu, Molecular dynamics simulations of effects of geometric parameters and temperature on mechanical properties of single-walled carbon nanotubes, *Journal of Composites Science* 8 (8) (2024).
- [12] M. Kumar, S. K. Tamang, A. Owhal, T. Roy, M. Dabi, Nano droplet behaviour on vibrating surfaces: atomistic simulations for bio-NEMS/MEMS applications, *Molecular Simulation* 50 (10) (2024) 644–652.
- [13] M. Čanađija, Deep learning framework for carbon nanotubes: Mechanical properties and modeling strategies, *Carbon* 184 (2021) 891–901.
- [14] V. Košmerl, I. Štajduhar, M. Čanađija, Predicting stress–strain behavior of carbon nanotubes using neural networks, *Neural Computing and Applications* 34 (20) (2022) 17821–17836.
- [15] M. Čanađija, V. Košmerl, M. Zlatić, D. Vrtovšnik, N. Munjas, A computational framework for nanotrusses: Input convex neural networks approach, *European Journal of Mechanics-A/Solids* 103 (2024) 105195.
- [16] D. Rogula, et al., Influence of spatial acoustic dispersion on dynamical properties of dislocations, *Bulletin de l’Académie Polonaise des Sciences, Séries des Sciences Techniques* 13 (1965) 337–343.
- [17] E. Kröner, Elasticity theory of materials with long range cohesive forces, *International Journal of Solids and Structures* 3 (5) (1967) 731–742.
- [18] D. Rogula, Introduction to nonlocal theory of material media, in: *Nonlocal theory of material media*, Springer, 1982, pp. 123–222.
- [19] A. C. Eringen, On differential equations of nonlocal elasticity and solutions of screw dislocation and surface waves, *Journal of Applied Physics* 54 (9) (1983) 4703–4710.

- [20] H. Kumar, S. Mukhopadhyay, Size-dependent thermoelastic damping analysis in nanobeam resonators based on Eringen's nonlocal elasticity and modified couple stress theories, *Journal of Vibration and Control* 29 (7-8) (2023) 1510–1523.
- [21] R. Barretta, M. Čanadija, F. Marotti de Sciarra, A higher-order Eringen model for Bernoulli–Euler nanobeams, *Archive of Applied Mechanics* 86 (2016) 483–495.
- [22] F. Ebrahimi, M. Dehghan, A. Seyfi, Eringen's nonlocal elasticity theory for wave propagation analysis of magneto-electro-elastic nanotubes, *Advances in Nano Research* 7 (1) (2019) 1–11.
- [23] G. Romano, R. Barretta, M. Diaco, F. Marotti de Sciarra, Constitutive boundary conditions and paradoxes in nonlocal elastic nanobeams, *International Journal of Mechanical Sciences* 121 (2017) 151–156.
- [24] G. Romano, R. Barretta, Nonlocal elasticity in nanobeams: the stress-driven integral model, *International Journal of Engineering Science* 115 (2017) 14–27.
- [25] G. Romano, R. Barretta, Stress-driven versus strain-driven nonlocal integral model for elastic nano-beams, *Composites Part B: Engineering* 114 (2017) 184–188.
- [26] G. Lovisi, Application of the surface stress-driven nonlocal theory of elasticity for the study of the bending response of FG cracked nanobeams, *Composite Structures* 324 (2023) 117549.
- [27] M. Altekin, E. E. Karatas, R. F. Y. (retired professor), Stress-driven nonlocal theory on nonlinear static analysis of annular nanoplates, *Mechanics Based Design of Structures and Machines* 53 (9) (2025) 6283–6328. [doi:10.1080/15397734.2025.2480706](https://doi.org/10.1080/15397734.2025.2480706).
- [28] R. Barretta, F. Fabbrocino, R. Luciano, F. Marotti de Sciarra, G. Ruta, Buckling loads of nano-beams in stress-driven nonlocal elasticity, *Mechanics of Advanced Materials and Structures* 27 (11) (2020) 869–875.
- [29] B. Das, D. Ussorio, M. S. Vaccaro, R. Barretta, R. Luciano, Dynamics of FG nanobeams on nonlocal medium, *Composite Structures* 366 (2025) 119057.

- [30] L. Feo, G. Lovisi, R. Penna, Free vibration analysis of functionally graded nanobeams based on surface stress-driven nonlocal model, *Mechanics of Advanced Materials and Structures* 31 (28) (2024) 10391–10399.
- [31] M. S. Vaccaro, R. Luciano, F. Marotti de Sciarra, Size-dependent stress-driven behaviour of nanobeams based on higher-order theories, *Meccanica* (2025). doi:<https://doi.org/10.1007/s11012-025-02004-3>.
- [32] D. Samadian, I. B. Muhit, N. Dawood, Application of data-driven surrogate models in structural engineering: a literature review, *Archives of Computational Methods in Engineering* 32 (2025) 735–784.
- [33] J. P. Stöcker, S. Heinzig, A. A. Khedkar, M. Kaliske, Data-driven computational mechanics: comparison of model-free and model-based methods in constitutive modeling, *Archive of Applied Mechanics* 94 (9) (2024) 2683–2718.
- [34] M. Zlatić, F. Rocha, L. Stainier, M. Čanadija, Data-driven methods for computational mechanics: a fair comparison between neural networks based and model-free approaches, *Computer Methods in Applied Mechanics and Engineering* 431 (2024) 117289. doi:<https://doi.org/10.1016/j.cma.2024.117289>.
- [35] J. N. Fuhg, G. Anantha Padmanabha, N. Bouklas, B. Bahmani, W. Sun, N. N. Vlassis, M. Flaschel, P. Carrara, L. De Lorenzis, A review on data-driven constitutive laws for solids, *Archives of Computational Methods in Engineering* 32 (2025) 1841–1883.
- [36] L. Yuan, Y.-Q. Ni, X.-Y. Deng, S. Hao, A-PINN: Auxiliary physics informed neural networks for forward and inverse problems of nonlinear integro-differential equations, *Journal of Computational Physics* 462 (2022) 111260.
- [37] M. Raissi, P. Perdikaris, G. Karniadakis, Physics-informed neural networks: A deep learning framework for solving forward and inverse problems involving nonlinear partial differential equations, *Journal of Computational Physics* 378 (2019) 686–707.
- [38] J. Han, A. Jentzen, W. E, Solving high-dimensional partial differential equations using deep learning, *Proceedings of the National Academy of Sciences* 115 (34) (2018) 8505–8510.



- [39] M. Mattheakis, D. Sondak, A. S. Dogra, P. Protopapas, Hamiltonian neural networks for solving equations of motion, *Physical Review E* 105 (6) (2022) 065305.
- [40] C. Flamant, P. Protopapas, D. Sondak, Solving differential equations using neural network solution bundles, *arXiv preprint arXiv:2006.14372* (2020).
- [41] S. Desai, M. Mattheakis, H. Joy, P. Protopapas, S. Roberts, One-shot transfer learning of physics-informed neural networks, *arXiv preprint arXiv:2110.11286* (2021).
- [42] G. E. Karniadakis, I. G. Kevrekidis, L. Lu, P. Perdikaris, S. Wang, L. Yang, Physics-informed machine learning, *Nature Reviews Physics* 3 (6) (2021) 422–440.
- [43] J. Yu, L. Lu, X. Meng, G. E. Karniadakis, Gradient-enhanced physics-informed neural networks for forward and inverse PDE problems, *Computer Methods in Applied Mechanics and Engineering* 393 (2022) 114823.
- [44] W. He, J. Li, X. Kong, L. Deng, Multi-level physics informed deep learning for solving partial differential equations in computational structural mechanics, *Communications Engineering* 3 (1) (2024) 151.
- [45] J. Sirignano, K. Spiliopoulos, DGM: A deep learning algorithm for solving partial differential equations, *Journal of Computational Physics* 375 (2018) 1339–1364.
- [46] H. Jin, M. Mattheakis, P. Protopapas, Unsupervised neural networks for quantum eigenvalue problems, *arXiv preprint arXiv:2010.05075* (2020).
- [47] H. Jin, M. Mattheakis, P. Protopapas, Physics-informed neural networks for quantum eigenvalue problems, in: *2022 International Joint Conference on Neural Networks (IJCNN)*, IEEE, 2022, pp. 1–8.
- [48] L. Harcombe, Q. Deng, Physics-informed neural networks for discovering localised eigenstates in disordered media, *Journal of Computational Science* 73 (2023) 102136.
- [49] I. Lagaris, A. Likas, D. Fotiadis, Artificial neural network methods in quantum mechanics, *Computer Physics Communications* 104 (1) (1997) 1–14.

- [50] L. Grubišić, M. Hajba, D. Lacmanović, Deep neural network model for approximating eigenmodes localized by a confining potential, *Entropy* 23 (1) (2021) 95.
- [51] J. Sadet, F. Massa, T. Tison, E.-G. Talbi, I. Turpin, Deep Gaussian process for the approximation of a quadratic eigenvalue problem: Application to friction-induced vibration, *Vibration* 5 (2) (2022) 344–369.
- [52] S. Yoo, M. S. Kang, H. Yoon, T. Kim, A physics-informed neural network approach for solving structural eigenvalue problem, *International Journal of Precision Engineering and Manufacturing* (2025). doi:<https://doi.org/10.1007/s12541-025-01280-z>.
- [53] A. Fallah, M. M. Aghdam, Physics-informed neural network for bending and free vibration analysis of three-dimensional functionally graded porous beam resting on elastic foundation, *Engineering with Computers* 40 (2024) 437–454.
- [54] T. Kapoor, H. Wang, A. Núñez, R. Dollevoet, Physics-informed neural networks for solving forward and inverse problems in complex beam systems, *IEEE Transactions on Neural Networks and Learning Systems* 35 (5) (2024) 5981–5995.
- [55] M. S. Vaccaro, F. P. Pinnola, F. Marotti de Sciarra, R. Barretta, Dynamics of stress-driven two-phase elastic beams, *Nanomaterials* 11 (5) (2021).
- [56] A. Fallah, M. M. Aghdam, Physics-Informed Neural Network for Solution of Nonlinear Differential Equations, 2024, pp. 163–178.
- [57] P. Ramachandran, B. Zoph, Q. V. Le, Searching for activation functions, arXiv preprint arXiv:1710.05941 (2017).
- [58] A. Al-Safwan, C. Song, U. B. Waheed, Is it time to swish? comparing activation functions in solving the Helmholtz equation using physics-informed neural networks, arXiv preprint arXiv:2110.07721 (2021).